Journal of Materials Chemistry C

PAPER

Cite this: J. Mater. Chem. C, 2015, 3, 1823

Facile synthesis of nanostructured carbon materials over RANEY® nickel catalyst films printed on Al_2O_3 and SiO_2 substrates†

Jhih-Fong Lin,[ab] Melinda Mohl,[a] Mikko Nelo,[a] Geza Toth,[a] Ákos Kukovecz,[cd] Zoltán Kónya,[ce] Srividya Sridhar,[f] Robert Vajtai,[f] Pulickel M. Ajayan,[f] Wei-Fang Su,[b] Heli Jantunen[a] and Krisztian Kordas*[a]

A quick and convenient approach that combines a printing process and chemical vapor deposition is developed for facile construction of nanostructured metal–carbon composite structures. Films of porous RANEY® nickel catalyst particles are deposited on various substrates by stencil printing from dispersions of the catalyst and poly(methyl methacrylate) in 2-(2-butoxyethoxy)ethyl acetate. After removing the organic binders at elevated temperatures, the mesoporous Ni film is applied as a growth template for synthesizing nanostructured carbon materials on the surface. Depending on the synthesis conditions, carbon nanofibers and nanotubes, as well as graphite deposits, are found to form on the substrates, allowing a robust and scalable production of carbon based inert electrodes of high specific surface area. In addition to structural characterization of the composites by means of scanning and transmission electron microscopy, Raman spectroscopy, X-ray diffraction, thermal gravimetric and surface adsorption analyses, the produced carbon/RANEY® nickel composites are also studied as electrodes in electrochemical capacitors (specific capacitance of ~12 F g^{-1}) and in field emitter devices with a low turn-on field (<1.0 V μm^{-1}). The results indicate the carbon/RANEY® nickel composites are suitable for direct integration on substrates used frequently in microelectronics.

Received 27th October 2014
Accepted 15th December 2014

DOI: 10.1039/c4tc02442g

www.rsc.org/MaterialsC

Introduction

In the past few decades, carbon nanomaterials of different dimensionality, such as fullerenes, carbon nanotubes and graphene, have been widely studied and employed in various applications. These carbon materials with the sp^2 atomic-bonding structure have high specific surface area, superior electrical and mechanical properties and are also light weight, making them truly multifunctional and particularly attractive for electrode applications. Since carbon nanotubes are typically synthesized on metal nanoparticles supported on oxides (typical diffusion barriers), direct application of the nanotubes for electrodes requires a number of different subsequent steps, including (i) functionalization and dispersion for inkjet printing conductive networks,[1,2] (ii) sputtering with metals for soldering aligned films[3] (iii) or dispersion and filtration for obtaining bucky papers.[4] Another approach to achieve carbon nanotube based electrodes is the direct growth of the nanotubes on conductive surfaces such as aluminum,[5,6] copper[7] or Inconel super-alloys.[8–11] Lately, three-dimensional porous networks of metal–carbon composites and hybrids have been proposed as potentially good candidates for electrodes in supercapacitors and field emitters.[12,13]

Ni nanoparticles have been long used to grow carbon nanotubes and various other carbonaceous species. In fact, Ni, which is an excellent catalyst for hydrogenation/dehydrogenation of hydrocarbons, has been applied by the petrochemical and food industries for nearly 100 years. Since its first successful synthesis in 1924, RANEY® nickel has been widely applied because of its high specific surface area (which can reach as high as 100 m^2 g^{-1}) and good hydrogen storage ability. One major difficulty of the catalyst is its relatively easy deactivation caused by coking (*i.e.* the formation of carbonaceous coating), which inhibits the reactants from adsorbing on the surface. For instance, the decomposition of acetylene on RANEY® nickel catalysts can produce different kinds of

[a]Microelectronics and Materials Physics Laboratories, Department of Electrical Engineering, University of Oulu, P.O. Box 4500, FI-90570 Oulu, Finland. E-mail: lapy@ee.oulu.fi
[b]Department of Materials Science and Engineering, National Taiwan University, 1, Roosevelt Road, Section 4, Taipei 106-17, Taiwan
[c]Department of Applied and Environmental Chemistry, University of Szeged, RerrichBelater 1, H-6720 Szeged, Hungary
[d]MTA-SZTE "Lendület" Porous Nanocomposites Research Group, RerrichBelater 1, H-6720 Szeged, Hungary
[e]MTA-SZTE Reaction Kinetics and Surface Chemistry Research Group, RerrichBelater 1, H-6720 Szeged, Hungary
[f]Department of Material Science and NanoEngineering, Rice University, Houston, Texas 77005, USA

† Electronic supplementary information (ESI) available. See DOI: 10.1039/c4tc02442g

carbonaceous materials such as filamentary or angular graphite laminae.[14] Two important factors were suggested to influence the production of nanofilamentary carbons. One is the appearance of distorted nickel particles at elevated temperature due to the partial melting of surficial nickel, while the other is associated with the local deposition of amorphous carbon to partially cover the catalyst. Such a partial poisoning of the catalyst (*i.e.* coking) results in location dependent decomposition of acetylene and consequently local temperature gradients, which has great importance in the localized dissolution and subsequent precipitation of carbon, referred to today as the vapor–liquid–solid growth model. Recent studies on the decomposition of methane over Ni nanoparticles and RANEY® type catalysts also indicate the efficiency of methane decomposition correlates with the production of carbon nanofilaments.[15,16] A number of different studies revealed that the size of Ni particles has a decisive role in the type of carbon forming on the catalyst. Increasing catalyst size results in less efficient carbon diffusion through the catalyst, giving rise to fiber formation instead of nanotubes (or in the extreme, poisoning the entire catalyst because of the growth of a carbon shell).[17,18]

In this work, we explore further the possibility of applying RANEY® Ni catalyst to grow Ni/carbon composites by immobilizing the catalyst material on solid wafers such as polycrystalline alumina and oxidized Si. We show that stencil printing of the catalyst is a feasible route to fabricate mesoporous RANEY® nickel templates for subsequent growth of nanostructured carbons by chemical vapor deposition. The integrated, electrically conductive, three-dimensional Ni/carbon composites of high specific surface area on solid substrates are feasible for supercapacitor and field-emitter electrodes and can be attractive for further hybrid electronics, especially for silicon on insulator (SOI) devices and for integrated microelectromechanical systems (MEMS).

Experimental

Preparation of RANEY® nickel paste and the stencil printing process

RANEY® 2400 nickel (slurry in water), poly(methyl methacrylate) (PMMA, M_W: 350 g mol^{-1}), 2-(2-butoxyethoxy)ethyl acetate ($C_{10}H_{20}O_4$, >99.2%) were purchased from Sigma-Aldrich and used without further purification. To make a catalyst paste for stencil printing, 88.0 g RANEY® nickel 2400 slurry is blended with 12.0 g poly(methyl methacrylate) (PMMA) in 100.0 g 2-(2-butoxyethoxy)ethyl acetate (>99.2%), and then mixed in ball-mill for overnight. After the milling process, small aliquots of acetone are used to transfer the paste from the ball-mill to a beaker. To remove acetone from the paste, the container is heated to 90 °C for about 15 min. The ready paste shows a typical non-Newtonian pseudoplastic fluid behavior with decreasing viscosity down to ~1.2 Pa s as the shear rate is increased (Fig. S1†).

In the stencil printing process, we apply a laser cut stainless steel mask (thickness of 100 μm) having square shaped patterns of 15 × 15 mm^2 size through which the paste is doctored with a lateral blade movement rate of ~1.0 m s^{-1}. Wafers of Si with 200 nm SiO_2 layer (Si-Mat silicon materials) and polycrystalline alumina (thickness of 0.25 mm, Laser Tech Services) were used as substrates. Before the stencil printing, thin films of titanium (40 nm) and nickel (100 nm) were deposited on the substrate by e-beam evaporation and magnetron sputtering, respectively, to ensure better adhesion of the catalyst and to help easy electrical interfacing of the grown structures in subsequent experiments. After the stencil printing process, the samples were annealed in a box furnace at 120 °C in ambient conditions for 15 min to remove the excess organic solvent (Scheme 1).

Synthesis of Ni/carbon composites

To grow CNTs and other carbonaceous materials, the patterned substrates were placed on a 2 inch size graphite heater in a cold-wall CVD reactor (Aixtron, Black Magic, UK). The samples were heated to the desired synthesis temperature (400, 600 or 800 °C with a heating rate 100 °C min^{-1}) in 500 sccm argon and 50 sccm hydrogen (5 mbar) and kept there for 30 minutes to facilitate the reduction of the catalyst. After this step, acetylene was introduced (flow rate of 10 sccm, at ~14 mbar) for a 20 min period to grow carbon, and then the samples were cooled in a flow of argon (500 sccm) and hydrogen (50 sccm) (Scheme 1).

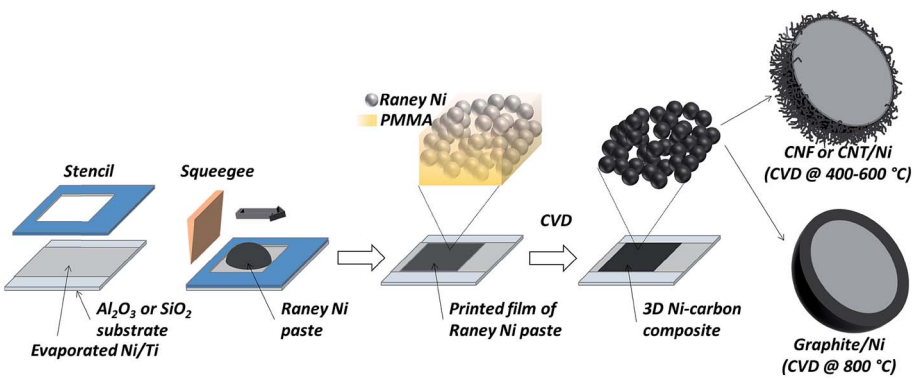

Scheme 1 Schematic of the fabrication process including evaporation of under-metallization, stencil printing the catalyst and subsequent chemical vapor deposition of nanostructured carbons.

Characterization

Powder X-ray diffraction (XRD) patterns of carbon/catalyst composites were characterized by Bruker D8 Discovery XRD system with Cu Kα radiation ($\lambda = 1.5418$ Å). The patterns were recorded in the scan range of $2\theta = 20$–$90°$ with a step size of 0.025° and a scan step of 4 s. To determine the quality of the synthesized carbon materials on the catalyst surface, Raman spectra of the products were assessed by a Horiba Jobin-Yvon Labram HR800 UV-vis μ-Raman instrument at $\lambda = 488$ nm excitation. To confirm the production yield of carbon on the nickel catalyst under different growth processes, the carbon/nickel composite products were collected from the substrate and characterized by thermal gravimetric analysis (TGA, Setaram Labsys) in air with a heating rate of 5 °C min^{-1} from room temperature to 1000 °C.

In the course of the surface adsorption analysis, the composites were preheated to 200 °C for 1 hour to desorb moisture, which was followed by nitrogen adsorption–desorption in a volumetric adsorption analyzer (Quantachrome Nova 3000E). The specific surface area was calculated by the multipoint BET equation and the pore volume was acquired from the adsorption curve at 0.96 relative pressure (calculation using software Quantachrome NovaWin). Morphology and microstructure of the synthesized materials are studied by the means of transmission (TEM, Leo 912 Omega) and field emission scanning electron microscopy (FESEM, Zeiss Ultra Plus).

Electrochemical capacitors were constructed from pairs of similar mesoporous composites as electrodes were separated by 2 layers of filter papers (Whatman 1, Cat no. 1001-047) used as spacers. The mixture of aqueous solution of KOH (6 M) and isopropyl alcohol with volume ratio 4 : 1 was applied as an electrolyte. Isopropyl alcohol was added to improve the wetting of the carbonaceous mesoporous electrode. The stack of electrodes and separators were mechanically clamped with a crocodile clip while performing cyclic voltammetry measurements (Princeton Applied Research VersaSTAT 3 potentiostat, voltage sweep rates of 0.05, 0.1, 0.25, and 0.5 V s^{-1}).

Results and discussion

Structure of the RANEY® nickel/carbon nanocomposites

After the growth processes at 400 °C, 600 °C, 800 °C, and 1000 °C, we observe various kinds of carbonaceous features forming nanostructured composites with the RANEY® catalyst (Fig. 1 and S2†). Upon growth at 400 °C or 600 °C, carbon filaments appear on the surface of RANEY® nickel catalysts. Synthesis at 800 °C results in far fewer filamentous products than seen at lower temperatures. TEM analysis reveals the filaments are mostly multi-walled carbon nanotubes in these samples (Fig. 2). In addition to nanotubes, graphitic deposits of 40–50 nm thickness are found on the catalyst for growth at 800 °C. Experiments carried out at 1000 °C made the porous catalyst structure collapse (Fig. S2†); thus, further experiments were not conducted.

As is typical in the vapor–liquid–solid (VLS) growth model for carbon nanotubes on metal catalyst, the dissociation of hydrocarbon molecules (to carbon atoms and clusters) is the first main step. It is a thermally activated process, proceeding in the gas phase but can be also catalyzed by the surface. After decomposition, the produced carbon species are adsorbed on

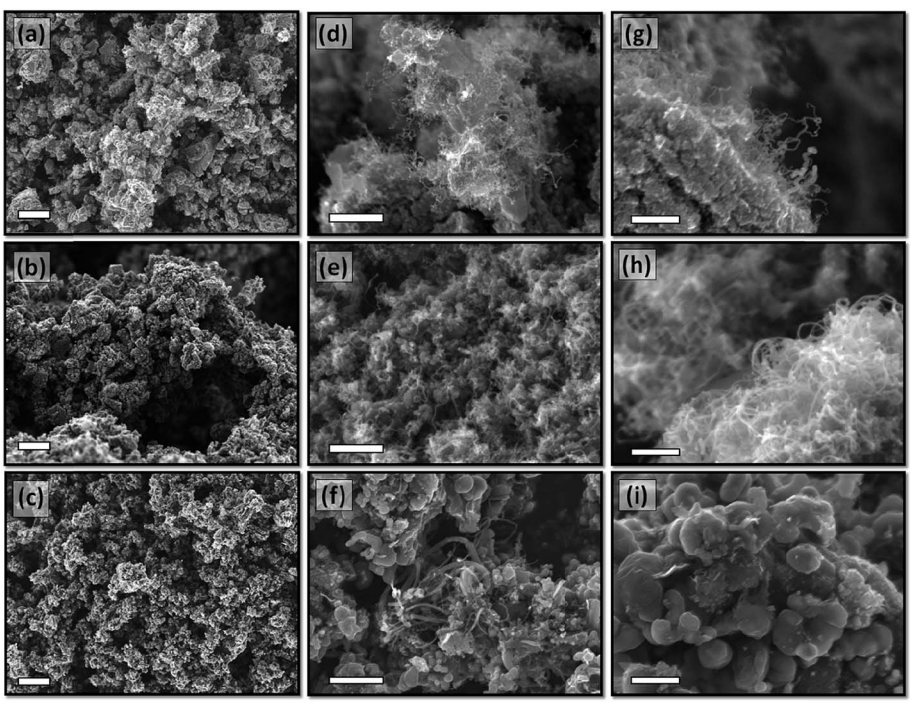

Fig. 1 SEM images of porous structure of carbon growth on nickel mesoporous layer at (a, d and g) 400 °C, (b, e and h) 600 °C, (c, f and i) 800 °C, the scale bar of (a–c), (d–f) and (g–i) are 10 μm, 1 μm and 400 nm, respectively.

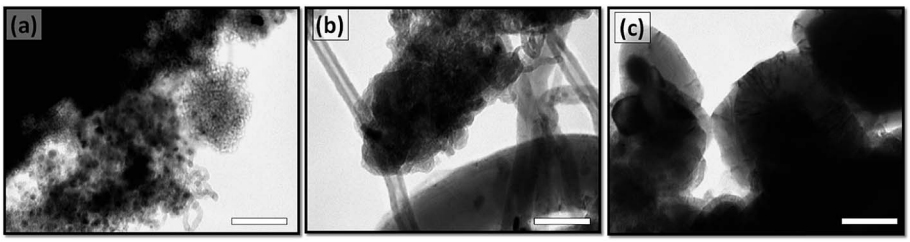

Fig. 2 TEM images of the carbon structure on the nickel mesoporous layer after (a) 400 °C, (b) 600 °C, and (c) 800 °C growth. The scale bars show 50 nm.

and dissolved in the catalyst particles. Since the solubility of carbon in metals highly depends on the surface curvature as well as on the temperature, minute fluctuations in such parameters can drive the carbon to phase separate (*i.e.* precipitate) and form carbonaceous deposits on the surface.[19] The process is highly influenced by the diffusion rate of carbon inside the catalyst (bulk diffusion model) or on the surface of the metal (surface diffusion model).[20,21] Based on the VLS model, we should observe rapid growth of CNTs at 800 °C because of the faster rate of hydrocarbon decomposition and enhanced carbon diffusion in the catalyst; however, the appearance of thick graphitic coating on the metal surface suggests a partial collapse of the mesoporous Ni structure, which is not favored for growing fibrous products. The massive precipitation of graphitic carbon layer on the surface is encapsulating the catalyst within a short period of time, thus blocking the surface.

X-ray powder diffraction measurements of the synthesized carbon/RANEY® nickel composites (Fig. 3a) show reflections around 44.2° and 51.5°, which correspond to (111) and (200) planes of face-centered cubic nickel, respectively. Peaks that could be assigned to nickel oxide are not observed in the diffraction patterns. The decreased peak broadening with temperature (Table 1) indicates a partial sintering of the metal, which supports our earlier explanation on the limited filament growth at 800 °C. The diffraction peak around 25.9° is due to the graphitic (002) planes being relatively intensive for the samples made at 600 °C (carbon nanotubes) and 800 °C (mainly graphite) as compared to those synthesized at 400 °C. Raman spectroscopy analyses of the samples (Fig. 3b) are in agreement with the XRD results. The ratio of the G and D band peak intensities (*i.e.* sp^2 graphitic ordering around 1580 cm^{-1} *vs.* sp^3 hybridized carbons or defects at around 1355 cm^{-1}) increases significantly from 1.0 to 3.4 for the materials grown at 400 °C and 800 °C, respectively (Fig. 4).

To further evaluate the production yield of carbon materials after the different growth temperatures, we employed thermogravimetric analysis (from 300 °C to 800 °C in air) to assess the mass fraction of synthesized carbon in the composites. The weight loss of 29.0%, 48.0% and 36.0% for the samples grown at 400 °C, 600 °C and 800 °C, respectively, indicates the optimum temperature for carbon growth is at 600 °C, in good accordance with the electron microscopy results shown earlier. On the other hand, it is worth mentioning that the degradation

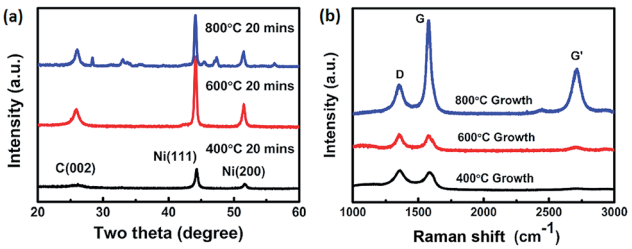

Fig. 3 (a) X-ray diffraction patterns and (b) Raman spectra for carbon on RANEY® nickel nanostructured composites.

Table 1 Summary of crystal properties and Raman spectra of different carbon/nickel composites

Growth temperature (°C)	Crystal size by Ni (111) (nm)	Crystal size by Ni (200) (nm)	Raman I_G/I_D
400	21.5	15.8	1.0
600	23.7	19.6	1.0
800	27.4	25.9	3.4

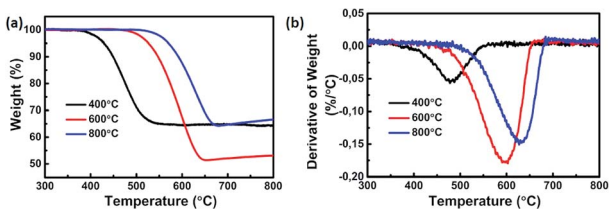

Fig. 4 (a) Weight and (b) differential thermal gravimetric curves for different nanostructured Ni/carbon composites.

temperature increases with the growth temperature of the composites. Such improvement is because of the better crystallinity of carbon in the structures grown at elevated temperatures, in good agreement with our Raman and XRD results.

Although electron microscopy and X-ray diffraction analyses suggested a gradual sintering of the catalyst at elevated temperatures, it is not clear how much the porous nature of the originally highly nanostructured catalyst is kept for the nickel/carbon composites. In order to assess any changes in the porosity and surface area, the synthesized samples were

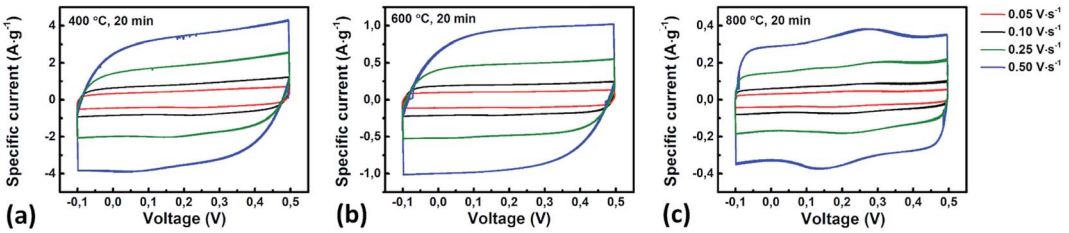

Fig. 5 Cyclic voltammetry curves with different charge/discharge rates of carbon grown on the nickel mesoporous layer after (a) 400 °C, (b) 600 °C, and (c) 800 °C growth process.

Table 2 Properties of carbon structure on RANEY® nickel mesoporous layer

Growth temperature (°C)	Specific surface area ($m^2\ g^{-1}$)	Pore volume ($cm^3\ g^{-1}$)	Carbon content (%)	Specific capacitance ($F\ g^{-1}$)
400	65.30	1.34×10^{-1}	29	12.3
600	35.90	6.90×10^{-2}	48	2.5
800	14.64	4.48×10^{-2}	36	1.0

subjected to surface adsorption analysis. According to the measurements, the specific surface area of RANEY® nickel (100 $m^2\ g^{-1}$) is decreased to approximately 65, 36 and 15 $m^2\ g^{-1}$ after carbon growth at 400 °C, 600 °C and 800 °C, respectively. On the other hand, the pore volume of the composites also decreases from 0.134 to 0.069 and 0.045 mL g^{-1} with increase in temperature (Fig. S3†).

RANEY® nickel/carbon nanocomposites as electrode materials

The porous structure with high carbon content and the presumably good electrical conductivity of the nickel/carbon nanocomposites, which are also immobilized on solid surfaces, suggest potential application of these materials for electrodes in supercapacitors and field emitters.

Cyclic voltammetry analysis (Fig. 5 and Table 2) of similar composite films in aqueous KOH electrolytes separated by cellulose membranes show rectangular CV curves with large hysteresis loops within a large voltage scan rate range (from 0.05 to 0.5 V s^{-1}), indicating the ideal capacitor behavior of the stacks. By dividing the saturation current density from the voltage–current curve with the voltage scan rate (0.25 V s^{-1}) and the weight of electrodes, the specific capacitance of the composites are 12.3 F g^{-1}, 2.5 F g^{-1} and 1.0 F g^{-1} (400 °C, 600 °C and 800 °C growth, respectively). Although the obtained specific capacitance values are not very high, the value measured for the sample grown at 400 °C is comparable with those reported for multi-walled carbon nanotubes (18 F g^{-1})[8] and (10–29 F g^{-1})[10] grown at 770 °C from ferrocene/xylene precursors. Both the decreased specific surface area and pore size of these electrodes explain well the lowered capacitance with the increasing growth temperature (Table 2).

Furthermore, these carbon/RANEY® nickel composite electrodes are also studied for cold cathodes for field emission. As shown in Fig. 6, the turn-on voltage (which is the field required to give a current density of 10 μA cm^{-2}) of three different electrodes are all below 0.9 V μm^{-1}, which is comparable with those measured for carbon nanobuds (0.65 V μm^{-1})[22] or for vertically aligned carbon nanotube arrays grown on Inconel (1.5 V μm^{-1} (ref. 11) and 1.2 V μm^{-1} (ref. 23)) or on Si (0.8 V μm^{-1} (ref. 22)) and significantly lower than that reported for screen printed carbon nanotubes (3 V μm^{-1} (ref. 24)).

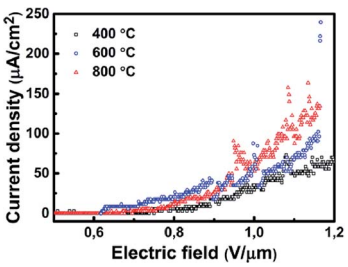

Fig. 6 Field emission of carbon/RANEY® nickel composites.

The carbon nanostructures we obtained on stencil printed Ni catalysts hold promise for integrated field emitters that, in principle, could be patterned with a print resolution of a few tens of micrometers after some optimization of the paste (adding surfactants and/or decreasing particle size),[25] as well as selecting other potentially feasible printing processes such as screen,[26] gravure[27] or inkjet,[28] instead of stencil printing. The method we described in this report may be optimized even further to allow entirely roll-to-roll compatible fabrication without the need for using vacuum processes. For instance, instead of the evaporated adhesion promoting under-metallization layers, one could apply thick-film printed conducting pastes consisting of some glass frit (binder between metal layer and substrate) before applying the RANEY® Ni pastes. Another approach could be a direct mixing of the glass frit into the

RANEY® Ni paste along with organic dispersants such that the catalyst is immobilized with enhanced adhesion on the substrate in a single deposition step.[29,30]

Conclusions

In summary, we developed a facile fabrication process for porous nanostructured metal–carbon composites by the combination of stencil printing and chemical vapor deposition processes. Patterns of catalyst films for subsequent growth of carbon nanomaterials (nanotubes, fibers and few layer graphite coatings) were obtained by stencil printing a RANEY® nickel based paste on alumina and SiO_2 substrates. The morphology of deposited carbon materials could be adjusted from nanofiber to nanotube and graphitic carbon layers by simply tuning the growth temperature. The nanostructured and porous carbon/nickel composites were found suitable for integrated electrochemical double-layer capacitor with specific capacitance up to 12.3 F g^{-1} as well as for cold cathode field emission electrodes with a turn-on field lower than 0.9 V μm^{-1}. Because stencil printing is a cost-effective and relatively simple method for depositing microscopic patterns of a number of different nanomaterials, we consider that the fabrication process reported in this study may be implemented and optimized further to fabricate supercapacitor and field emitter electrodes, as well as other components for applications in microelectronics, even in bulk quantities.

Acknowledgements

We thank Elina Jansson (VTT Technical Research Centre of Finland) for her help in viscosity measurements. The financial support of the M-ERA.NET (VOCSENSOR, OTKA, NN 110676), Academy of Finland (Suplacat and Optifu) and EU FP7 (Susfoflex, 289829 and Hippocamp, 608800) projects are acknowledged.

References

1 K. Kordas, T. Mustonen, G. Toth, H. Jantunen, M. Lajunen, C. Soldano, S. Talapatra, S. Kar, R. Vajtai and P. M. Ajayan, *Small*, 2006, **2**, 1021.
2 E. Gracia-Espino, G. Sala, F. Pino, N. Halonen, J. Luomahaara, J. Maklin, G. Toth, K. Kordas, H. Jantunen, M. Terrones, P. Helisto, H. Seppa, P. M. Ajayan and R. Vajtai, *ACS Nano*, 2010, **4**, 3318.
3 G. Toth, J. Maklin, N. Halonen, J. Palosaari, J. Juuti, H. Jantunen, K. Kordas, W. G. Sawyer, R. Vajtai and P. M. Ajayan, *Adv. Mater.*, 2009, **21**, 2054.
4 M. Kaempgen, M. Lebert, N. Nicoloso and S. Roth, *Appl. Phys. Lett.*, 2008, **92**, 094103.
5 R. Ummethala, V. O. Khavrus, A. Leonhardt, B. Buchner and J. Eckert, *Chem. Vap. Deposition*, 2012, **18**, 326.
6 C. Emmenegger, P. Mauron, A. Zuttel, C. Nutzenadel, A. Schneuwly, R. Gallay and L. Schlapbach, *Appl. Surf. Sci.*, 2000, **162**, 452.
7 G. Atthipalli, Y. Tang, A. Star and J. L. Gray, *Thin Solid Films*, 2011, **520**, 1651.
8 S. Talapatra, S. Kar, S. K. Pal, R. Vajtai, L. Ci, P. Victor, M. M. Shaijumon, S. Kaur, O. Nalamasu and P. M. Ajayan, *Nat. Nanotechnol.*, 2006, **1**, 112.
9 K. Aitola, J. Halme, N. Halonen, A. Kaskela, M. Toivola, A. G. Nasibulin, K. Kordas, G. Toth, E. I. Kauppinen and P. D. Lund, *Thin Solid Films*, 2011, **519**, 8125.
10 N. Halonen, J. Maklin, A. R. Rautio, J. Kukkola, A. Uusimaki, G. Toth, L. M. Reddy, R. Vajtai, P. M. Ajayan and K. Kordas, *Chem. Phys. Lett.*, 2013, **583**, 87.
11 S. Sridhar, L. Ge, C. S. Tiwary, A. C. Hart, S. Ozden, K. Kalaga, S. Lei, S. V. Sridhar, R. K. Sinha, H. Harsh, K. Kordas, P. M. Ajayan and R. Vajtai, *ACS Appl. Mater. Interfaces*, 2014, **6**, 1986.
12 Z. Yan, L. L. Ma, Y. Zhu, I. Lahiri, M. G. Hahm, Z. Liu, S. B. Yang, C. S. Xiang, W. Lu, Z. W. Peng, Z. Z. Sun, C. Kittrell, J. Lou, W. B. Choi, P. M. Ajayan and J. M. Tour, *ACS Nano*, 2013, **7**, 58.
13 Z. J. Fan, J. Yan, L. J. Zhi, Q. Zhang, T. Wei, J. Feng, M. L. Zhang, W. Z. Qian and F. Wei, *Adv. Mater.*, 2010, **22**, 3723.
14 R. T. K. Baker, M. A. Barber, P. S. Harris, F. S. Feates and R. J. Waite, *J. Catal.*, 1972, **26**, 51.
15 N. Mahata, A. F. Cunha, J. J. M. Orfao and J. L. Figueiredo, *Appl. Catal., A*, 2008, **351**, 204.
16 A. F. Cunha, J. J. M. Orfao and J. L. Figueiredo, *Appl. Catal., A*, 2008, **348**, 103.
17 H. Y. Wang and A. C. Lua, *J. Phys. Chem. C*, 2012, **116**, 26765.
18 M. Chhowalla, K. B. K. Teo, C. Ducati, N. L. Rupesinghe, G. A. J. Amaratunga, A. C. Ferrari, D. Roy, J. Robertson and W. I. Milne, *J. Appl. Phys.*, 2001, **90**, 5308.
19 N. Halonen, K. Kordas, G. Toth, T. Mustonen, J. Maklin, J. Vahakangas, P. M. Ajayan and R. Vajtai, *J. Phys. Chem. C.*, 2008, **112**, 6723.
20 S. Hofmann, C. Ducati, J. Robertson and B. Kleinsorge, *Appl. Phys. Lett.*, 2003, **83**, 135.
21 O. Pitkanen, N. Halonen, A.-R. Leino, J. Maklin, A. Dombovari, J.-F. Lin, G. Toth and K. Kordas, *Top. Catal.*, 2013, **56**, 522.
22 A. G. Nasibulin, P. V. Pikhitsa, H. Jiang, D. P. Brown, A. V. Krasheninnikov, A. S. Anisimov, P. Queipo, A. Moisala, D. Gonzalez, G. Lientschnig, A. Hassanien, S. D. Shandakov, G. Lolli, D. E. Resasco, M. Choi, D. Tomanek and E. I. Kauppinen, *Nat. Nanotechnol.*, 2007, **2**, 156.
23 S. Sridhar, C. Tiwary, S. Vinod, J. J. Taha-Tijerina, S. Sridhar, K. Kalaga, B. Sirota, A. H. C. Hart, S. Ozden, R. K. Sinha, Harsh, R. Vajtai, W. Choi, K. Kordás and P. M. Ajayan, *ACS Nano*, 2014, **8**, 7763.
24 J. T. Li, W. Lei, X. B. Zhang, X. D. Zhou, Q. L. Wang, Y. N. Zhang and B. P. Wang, *Appl. Surf. Sci.*, 2003, **220**, 96.
25 Y. L. Wu, Y. N. Li, P. Liu, S. Gardner and B. S. Ong, *Chem. Mater.*, 2006, **18**, 4627.
26 J. E. Jung, Y. W. Jin, J. H. Choi, Y. J. Park, T. Y. Ko, D. S. Chung, J. W. Kim, J. E. Jang, S. N. Cha, W. K. Yi,

S. H. Cho, M. J. Yoon, C. G. Lee, J. H. You, N. S. Lee and J. B. Yoo, *Phys. B*, 2002, **323**, 71.
27 M. Pudas, J. Hagberg and S. Leppavuori, *IEEE Trans. Electron. Packag. Manuf.*, 2002, **25**, 335.
28 J. J. Schneider, J. Engstler, S. Franzka, K. Hofmann, B. Albert, J. Ensling, P. Gutlich, P. Hildebrandt, S. Dopner, W. Pfleging, B. Gunther and G. Muller, *Chem.–Eur. J.*, 2001, **7**, 2888.
29 S. B. Rane, T. Seth, G. J. Phatak, D. P. Amalnerkar and M. Ghatpande, *J. Mater. Sci.*, 2004, **15**, 103.
30 C. Ballif, D. M. Huljić, G. Willeke and A. Hessler-Wyser, *Appl. Phys. Lett.*, 2003, **82**, 1878.